Asian Journal of Chemistry; Vol. 34, No. 10 (2022), 2611-2622

ASIAN JOURNAL OF CHEMISTRY

https://doi.org/10.14233/ajchem.2022.23867

Design, Synthesis, Theoretical, Spectroscopic and Molecular Docking Studies of Ruthenium and Zinc Complexes and their Antimycobacterial Study

ASHOK KUMAR SINGH[1,*], LOVELY KUMARI[1], KAVITA DHARIYAL[1], FARHA ARSHI[1], SUDHEER KUMAR SINGH[2], ABHISHEK KHARE[3] and AMARENDRA KUMAR[3]

[1]Department of Chemistry, Lucknow University, Lucknow-226007, India
[2]Department of Microbiology, Central Drug Research Institute, Lucknow-226031, India
[3]Departments of Physics, Lucknow University, Lucknow-226007, India

*Corresponding author: E-mail: singhaks3@rediffmail.com

Received: 9 April 2022; *Accepted*: 19 June 2022; *Published online*: 19 September 2022; AJC-20964

The six mononuclear complexes of ruthenium and zinc *viz*. [Ru(bpy)$_2$(HL1)]Cl (ML1), [Ru(bpy)$_2$(HL2)]Cl (ML2), [Ru(bpy)$_2$(HL3)]Cl (ML3), [ZnCl(H$_2$O)HL1]Cl (ML4), [ZnCl(H$_2$O)HL2]Cl (ML5), [ZnCl(H$_2$O)HL3]Cl (ML6); bpy = 2,2′-bipyridyl, HL = substituted thiosemicarbazone: HL1 = Cl, HL2 = OCH$_3$, HL3 = OCH$_2$Ph) were synthesized and characterized by elemental analysis, IR, ^{1}H and ^{13}C NMR, UV-Vis and ESI-MS spectroscopy techniques. The gas phase geometries of all the complexes have been optimized by density functional theory (DFT). The antimycobacterial activity of all the compounds was performed initially at 100 µM concentration, followed by MIC determination studies with compounds, which showed 90% reduction in fluorescence intensity. In addition, molecular docking analysis was performed to know the interactions between complexes and their probable binding sites in penicillin binding protein (PBP2). The 90% reduction in fluorescence intensity of the mycobacterial cultures were observed with HL2, HL3 and ML3. The MIC determination study showed good inhibition of ML3 and HL3 treated cultures even at 25 µM concentration. The potential activity shown by HL3 and ML3 cultures shows to be promising compounds, which may be further optimized for improved antimycobacterial activity. Electronic properties and various reactivity descriptors have been determined theoretically and an attempt has been perform to establish the correlation between biological activity and these parameters for the concerned metal complexes.

Keywords: Anti-mycobacterial activity, Fluorescence, Optimization, Ruthenium(II) bipyridyl, Docking.

INTRODUCTION

Mycobacterium spp. includes the pathogenic bacteria causing tuberculosis in humans and also leprosy. They are detrimental to the people, especially immuno-compromised like having AIDS or on immune suppressing medications [1]. Tuberculosis (TB) caused by *Mycobacterium tuberculosis* (*Mtb*) caused almost 1.5 million deaths in a year 2019 including close to 0.251 million deaths caused by HIV-TB [2]. In view of emerging drug resistance scenario, design and development of new drugs to treat tuberculosis are required. *Mycobacterium tuberculosis* H37Ra (*Mtb*-Ra) is a virulent strain of *Mtb* that can be suitably employed to test efficacy of new inhibitors. The resazurinmicrotiter plate assay (REMA) is very cost-effective for use in antimycobacterial efficacy testing. The Au(II)-NHC complexes have been extensively developed as potential chemotherapeutic agents [3]. The ligand plays key role in the development of compounds, which in turn can offer broad spectrum antimycobacterial activities. The Werner type silver(I) complexes showed antimicrobial activities, based on the molecular structure [4].

The accomplishment of cisplatin and related analogues platinum based complexes as anticancer agents had encouraged researchers to investigate other active transition metal complexes and in particular ruthenium as an alternative to platinum based anticancer compounds [5]. The ruthenium based complexes containing nitrogen and oxygen donor ligands are found to be effective against mycobacterium [6]. Further, the oxidation state of the ruthenium center is decided by the coordination surroundings ruthenium, plays a pivotal role in stabilizing its various oxidation states [7,8]. Ruthenium complexes are considered as promising alternative to platinum based

complexes and provide many approaches to innovative metal-based drugs. The tuning in the ligand environment is accompanied by a steady rise in the biological effects which ruthenium based complexes can exert [5,9]. Ruthenium compounds are regarded as expected alternatives to platinum compounds and offer many biocompatible to innovative metal based drugs.

Although, several promising results had been reported, the mononuclear polypyridyl metal complexes had still not further declared as therapeutic agents. This may be due to the development of a large number of antibiotics in the 1960s as well as a lower incidence of drug resistance at that time. In last few years, zinc and ruthenium compounds bearing thiosemicarbazide ligands which offered *in vivo* anticancer and *in vitro* antibacterial activity have been carried out. In this work, the synthesis and characterization of some ruthenium and zinc complexes and their antimycobacterial activity are discussed. Finally, molecular docking analysis was also performed to elucidate the mode of action of these compounds, to support the effective binding of molecules at the active site of protein (penicillin binding proteins (PBPs) [10-14]. Penicillin-binding proteins play a paramount role in the bacterial cell cycle, by catalyzing the *trans*-peptidation reaction in cell wall construction. Penicillin-binding proteins (PBPs) are a group of proteins that are characterized by their affinity for and binding of penicillin. They are a normal constituent of many bacteria; the name just reflects the way by which the protein was discovered. All β-lactam antibiotics (except for tabtoxinine-β-lactam) which inhibit glutamine synthesase) bind to PBPs, which are essential for bacterial cell wall synthesis. PBPs are members of a subgroup of enzymes called transpeptidase and specifically, these are DD-transpeptidases. PBPs are all involved in the final stages of the synthesis of peptidoglycan, which is the major component of bacterial cell walls. Bacterial cell wall synthesis is essential to growth, cell division (thus reproduction) and maintaining the cellular structure in bacteria [15]. Inhibition of PBPs leads to defects in the cell wall structure and irregularities in cell shape, for example filamentation, pseudomulticellular forms, lesions leading to spheroplast formation and eventual cell death and lysis [16]. PBPs bind to β-lactam antibiotics because they are similar in chemical structure to the modular pieces that form the peptidoglycan [17]. When they bind to penicillin, β-lactam amide bond is ruptured to form a covalent bond with the catalytic serine residue at the PBPs active site. This is an irreversible reaction and inactivates the enzyme. There has been a great deal of research into PBPs because of their role in antibiotics and resistance. Bacterial cell wall synthesis and the role of PBPs in its synthesis is a very good target for drugs of selective toxicity because the metabolic pathways and enzymes are unique to bacteria [18].

EXPERIMENTAL

All the LR chemicals were procured from Merck and used as received. The melting point of ligand and metal complexes was taken in the open capillary and are uncorrected. NMR spectra were recorded on a Bruker Avance IIIHD Spectrometer, FT-IR spectra were obtained in KBr pallet in the 4000-400 cm^{-1} region on a Fourier transform infrared spectrophotometer-8400 Shimadzu, electronic spectra on UV-Vis spectrophotometer Labtronic-2900, Mass spectra were recorded on a GCMS-QP2010 Shimadzu & micromass Q-T of Micro, elemental analysis was carried out on EURO EA Elemental Analyzer, EA-3000, RS-232. The conductivities of all complexes were obtained on ESICO microprocessor based conductivity/TDS meter model-1601. To optimize the structure and calculate the electronic structure properties of all the metal complexes, the density functional theory has been employed using Becke's three parameter hybrid exchanges functional with Lee-Yang-Parr correlation functional and the 6-31G(d,p) and for Ru and Zn atoms LANL2DZ were used as a basis set [19-25]. Gaussian 09 programs have been used to perform the calculations [26]. The frequencies were determined to confirm the minimum energy structure which is validated by the absence of imaginary wavenumbers on the calculated vibrational spectrum. Since DFT hybrid B3LYP functional tend to overestimate the fundamental modes, the vibrational frequencies are scaled down by the proper factor [27,28]. The assignments of vibrational wave number have been completed by combining the results of the Gauss View 5 program, symmetry considerations and the VEDA 4 program [29,30]. Dipole moment (μ) and mean polarizability (α) have also been calculated based on finite field approach using the density functional theory. Following Buckingham's definitions, the total dipole moment and the mean polarizability in a Cartesian frame is defined by $\mu = (\mu_x^2 + \mu_y^2 + \mu_z^2)^{1/2}$ and $\alpha = 1/3\ [\alpha_{xx} + \alpha_{yy} + \alpha_{zz}]$, respectively. In order to understand better the effectiveness of the ligand and complexes, molecular docking was performed [31]. The software used to predict the binding affinity of compounds was Auto Dock 4.2 [32]. For molecular docking calculations, the crystal structures of enzymes were downloaded from the Royal Collaboratory for Structural Bioinformatics, RCSB Protein Data Bank (http://www.rcsb.org/pdb/) [33]. Water molecules and co-crystallized ligands were removed from the .pdb. The structure of Zn and Ru complexes was drawn and optimized using Avogadro 1.2.0. [34]. In order to perform molecular docking for the ligand and the ruthenium and zinc complexes, their optimized geometry was used. Preparation of the compounds and proteins, polar hydrogen atoms and partial charges (Kollman and Gasteiger charges) were performed using Auto Dock Tools 1.5.6 that saved them as pdbqt [32]. It is based on algorithms that by setting the grid box are able to predict compound poses within the protein target and to assess them by scoring functions. The spacing dimensions of the grid were 1 Å. The three dimensional results of the interactions between the target and compound were analyzed and illustrated with PyMOL software [35,36].

Antimycobacterial drug susceptibility testing: The Resazurin microtiter plate assay, with acetate as a carbon source was used for antimycobacterial drug susceptibility test (DST) [37,38]. The details are *Mycobacterium tuberculosis* H37Ra (*Mtb*-Ra) log phase culture growing in Sauton's medium, was pelleted and washed twice with Sauton's medium provided with acetate instead of glycerol. Afterwards, the pellet was diluted in this acetate containing medium to $OD_{600} = 0.10$ and 100 μL cells were transferred to 96-well microtiter plate followed by the addition o 100 μL Sauton's medium (with acetate).

Compound concentration was adjusted initially to 100 µM. The assay controls for sterility, solvent and growth were also set-up. All the experiments were performed in triplicates. The plates were kept at 37 ºC for 5 days and subsequently 25 µL of resazurin (0.03% w/v) was added. After 5 h, fluorescence was recorded (535/595 nm excitation/emission) using a BMG Omega fluorescence plate reader. For MIC determination, compounds were serially diluted two-fold from 100 to 3.125 µM (100, 50, 25, 12.5, 6.25 and 3.125). The MIC_{90} was the concentration, which caused 90% or more reduction in fluorescence of *Mtb*-Ra culture.

Synthesis of ligands: The chalcones were synthesized by the addition of equimolar quantity of appropriately ethanolic solution of chloro, methoxy and benzyloxybenzaldehydes (0.01 mol) and 2-hydroxy acetophenone (0.01 mol) in 15-30 mL of ethanol and then the mixture was allowed to stir for 20 min. Further, 10 mL of 40% aqueous KOH solution was slowly added dropwise to the reaction mixture [39]. The reaction solution was allowed to stir at room temperature for approximately 1 h. The precipitate formed was then collected by filtration and recrystallized in methanol. Further, ethanolic solution of chloro (0.001 mol, 0.091 g), methoxy (0.001 mol, 0.270 g), benzyloxy (0.001 mol, 0.330 g) chalcones were reacted with thiosemicarbazide (0.001 mol, 0.091 g) in presence of KOH (0.025 mol) and refluxed in ethanol (25-30 mL) for 8 h. The solution was poured into ice-water. The precipitate was filtered and recrystallized from methanol. The resulting ligands were isolated as chloro-thiosemicarbazone (HL1), methoxy-thiosemicarbazone (HL2) and benzyloxy-thiosemicarbazone (HL3).

(*E*)-2-((*E*)-3-(4-(Chloro)phenyl)-1-(3-nitrophenyl)-allylidene)hydrazinecarbothioamide (HL1): Colour: brown solid: yield: (190 mg, 82%); m.p.: 193-195 ºC; UV-Vis (ethanol, 10^{-3} M, λ_{max}, nm): 244, 340; FT-IR (KBr, ν_{max}, cm^{-1}): 3432.48 (NH_2), 2745.79 (CH imines), 1694.54 (NH bend.), 1513.22 (C=N), 1381.09 (C=S), 841.96 (Ar-Cl); ^{1}H NMR (DMSO-d_6, 300 MHz) δ (ppm): 10.42 (1H, s, NH), 7.80 (2H, s, NH_2), 7.19 (2H, d, CH=CH), 8.85 (1H, s, $ArCHNO_2$), 8.49 (2H, d, ArCHCl), 8.70 (2H, d, ArCHCl). ^{13}C NMR (DMSO-d_6, 300 MHz) δ (ppm): 187.95 (C=S), 148.71 (C=N), 144.52 (C-NO_2), 122.61 (=CH), 127.94 (=CH). Anal. calcd. (found) % for $C_{16}H_{13}N_4O_2SCl$: C, 53.26 (52.96); H, 3.63 (3.60); N, 15.53 (15.03), S, 8.88 (8.83).

((*E*)-2-((*E*)-3-(4-(Methoxy)phenyl)-1-(3-nitrophenyl)-allylidene)hydrazinecarbothioamide (HL2): Colour: Dull brown crystalline solid; Yield: (191 mg, 84%); m.p.: 172-175 ºC); UV-Vis (ethanol, 10^{-3} M, λ_{max}, nm): 250, 340; FT-IR (KBr, ν_{max}, cm^{-1}): 3416.18 (NH_2, NH *str.*), 2361.94 (CH imines), 1598.09 (NH bend.), 1511.29 (C=N), 1340.90 (C=S), 1170.84 (Ar-O-CH_3); ^{1}H NMR (DMSO-d_6, 300 MHz) δ (ppm): 9.96 (1H, s, NH), 7.82 (2H, d, CH=CH), 7.79 (2H, s, NH_2), 8.82 (1H, s, ArCH-NO_2), 8.07-8.47 (2H, d, ArCH-OCH_3), 3.83 (3H, s, -OCH_3); ^{13}C NMR (DMSO-d_6, 300 MHz) δ (ppm): 187.81 (C=S), 148.67 (C=N), 146.15 (C-NO_2), 127.65 (=CH), 123.21 (=CH), 55.91 (C-OCH_3). Anal. calcd. (found) % for $C_{17}H_{16}N_4O_3S$ (*m.w.*: 356.09): C, 57.29 (57.19); H, 4.52 (5.14); N, 15.72 (15.69); S, 8.98 (8.86).

(*E*)-2-((*E*)-3-(4-(Benzyloxy)phenyl)-1-(3-nitrophenyl)-allylidene)hydrazinecarbothioamide (HL3): Colour: Dark brown powder, Yield: (272 mg, 87%); m.p.: 184-186 ºC; UV-Vis (ethanol, 10^{-3} M, λ_{max}, nm): 240, 350; FT-IR (KBr, ν_{max}, cm^{-1}): 3418.97 (NH_2, NH *str.*), 3035.12 (CH imines), 1602.91 (NH bend.), 1507.43 (C=N), 1375.30 (C=S), 1233.53, (OCH_2); ^{1}H NMR ((DMSO-d_6, 300 MHz) δ (ppm): 9.00 (1H, s, NH), 7.17 (2H, d, CH =CH), 7.40 (2H, s, NH_2), 8.57 (1H, s, ArCH-NO_2), 7.17, 7.14 (2H, d, ArCH-OCH_3), 5.03 (2H, s, OCH_2); ^{13}C NMR (DMSO-d_6, 300 MHz) δ (ppm): 167.15 (C=S), 129.85 (C=N), 128.42 (C=CH_2), 125.22 (=CH), 115.05 (=CH), 63.21 ($OCH_2C_6H_5$). Anal. calcd. (found) % for $C_{23}H_{20}N_4O_3S$ (*m.w.*: 432.13): C, 63.87 (62.59); H, 4.66 (5.16); N, 12.95 (14.39); S, 7.40 (7.09).

Synthesis of metal complexes: The $Ru(bpy)_2Cl_2$ was synthesized by dissolving $RuCl_3 \cdot 3H_2O$, (0.25 mol, 1.00 g) and 2,2′-bipyridyl (0.50 mol, 0.780 g) in 50 mL DMF and refluxed for 3 h in inert condition. The reddish-brown solution was slowly turned purple and the product was isolated from the reaction mixture. The solution was frozen overnight at 0 ºC. A microcrystalline mass was filtered and the residue was repeatedly washed with 30% LiCl solution and finally recrystallized from ethanol. The product was dried and stored in vacuum desiccators over P_2O_5 for further use (yield 75%). A hot ethanol solution of the respective ligands HL1-HL3 (0.1 mol) were mixed with an ethanol solution of Ru(II) 2,2′-bipyridyl (0.1 mol, 0.413 g) and the mixture was refluxed on an oil bath for 4 h and then cooled to room temperature. Further, the ligands HL1-HL3 was reacted with ethanol solution of $ZnCl_2 \cdot 2H_2O$ and refluxed for 2 h. On cooling, a coloured solid product was formed. The solid was filtered, washed with ethanol, then diethyl ether and dried. Crystallization from ethanol gave the desired metal complexes (**Scheme-I**).

[Ru(bpy)$_2$(HL1)]Cl(ML1): Complex **ML1** was synthesized by refluxing [Ru(II)$(bpy)_2Cl_2$] (0.25 mol, 1.251 g) and HL1 (0.25 mol, 1.794 g) in 100 mL of ethanol for 6 h under nitrogen atmosphere. The volume of the solution was reduced to 20 mL by rotatory evaporator and kept overnight. The dark brown powder was isolated and recrystallized in ethanol and collected by filtration, washed by diethyl ether and dried in a vacuum. Colour: brownish black powder; Yield: (94.5 mg, 53%); m.p.: > 250 ºC; UV-Vis (ethanol, 10^{-3} M, λ_{max}, nm): 233, 311, 363 and 512sh; FTIR (KBr, ν_{max}, cm^{-1}): 2835.36 (CH imines), 3005.10 (NH_2), 1600.92 (NH), 1145.72 (N-N), 1510.26 (C=N), 665.44 (C-S); 420.48 (Ru-N and Ru-S);^{1}H NMR (DMSO-d_6, 300 MHz) δ (ppm): 10.00 (1H, s, NH), 7.66 (2H, d, CH=CH), 8.52 (2H, s, NH_2). ^{13}C NMR (DMSO-d_6, 300 MHz) δ (ppm): 187.94 (C=S), 144.52 (C=N), 148.70 (C-NO_2), 122.61 (=CH), 127.94 (=CH); ESI/MS (methanol) calcd. (found) *m/z*: 803.04, (803.04, M^+). Anal. calcd. (found) % for $C_{38}H_{34}N_8O_2SRuCl_2$ (*m.w.* 774.32): C, 54.41 (54.38); H, 4.09 (4.04); N, 13.36 (13.32); S, 3.82 (3.78).

[Ru(bpy)$_2$(HL2)]Cl (ML2): Complex **ML2** was prepared by dissolving [Ru$(bpy)_2Cl_2$] (0.25 mol, 1.250 g) and HL2 (0.25 mol, 0.171 g) in ethanol (100 mL) and refluxed on oil bath for 4 h under N_2 atmosphere. The volume of the solution was reduced to 20 mL by rotator evaporator and kept overnight. The black powder was isolated and recrystallized in ethanol. The respective complex was filtered and washed by diethyl

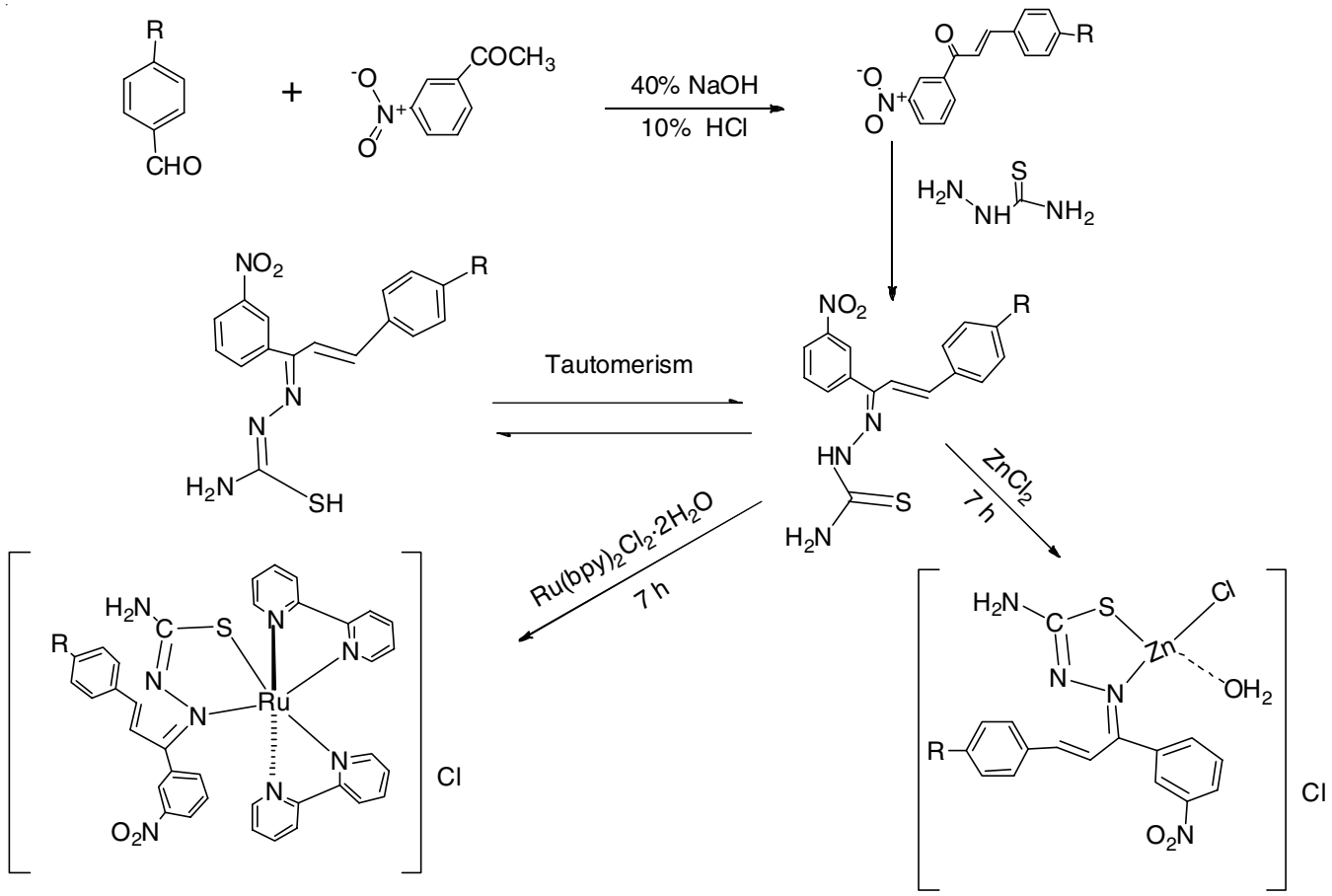

R = Cl (M1R, M4R), OCH_3 (M2R, M5R), OCH_2Ph (M3R, M6R)

Scheme-I: Synthetic routes for the preparation of the ligand and complexes

ether and dried in vacuum. Colour: Dull black powder, Yield: (97.5 mg, 55%); m.p.: > 250 ºC, UV-Vis (ethanol, 10^{-3} M, λ_{max}, nm): 233, 310, 381 and 506sh; FTIR (KBr, ν_{max}, cm^{-1}): 3214.51 (NH_2 and NH *str.*), 2362.90 (CH imines), 1607.44 (NH bend.), 1475.61 (C=N *str.*), 1416.78 (C-N *str.*), 1346.37 (C=S *str.*), 622.07 (C-S, *str.*), 503.44 (Ru-N and Ru-S); ^{1}H NMR (DMSO-d_6, 300 MHz) δ (ppm): 11.38 (1H, s, NH), 4.47 (2H, s, CH=CH), 7.79 (2H, s, NH_2), 3.45 (OCH_3), 3.83 (3H, s, -OCH_3); ^{13}C NMR (DMSO-d_6, 300 MHz) δ (ppm): 195.71 (C=S), 136.91 (C=N), 151.32 (CNO_2), 45.60 ($COCH_3$), 114.93 (=CH), 115.09 (=CH). ESI/MS (methanol), calcd. (found) *m/z*: 799.14 (799.15, M^+). Anal. calcd. (found) % for $C_{39}H_{37}N_8O_3SRu$ (*m.w.* 758.90): C, 56.14 (56.09); H, 4.47 (4.38); N, 13.43 (13.39); S, 3.84 (3.82).

[Ru(bpy)$_2$(HL3)]Cl (ML3): Complex **ML3** was synthesized by refluxing of [Ru(bpy)$_2$Cl$_2$] (0.25 mol, 1.251 g) and HL3 (0.25 mol, 2.395 g) in ethanol (100 mL) under inert atmosphere for 4 h. The resulting solution was reduced to 20 mL by rotator evaporator and kept overnight. The dark blackish brown powder was precipitated and filtered, washed by diethyl ether and dried in vacuum. Colour: Dark blackish brown powder; Yield: (115.8 mg, 59%); m.p.: > 250 ºC; UV-Vis (ethanol, 10^{-3} M, λ_{max}, nm): 231, 313, 426 and 506sh; FTIR (KBr, ν_{max}, cm^{-1}): 3869.20 (NH_2 and NH *str.*), 3739.97 (C-H *str.* arom.), 2953.02 (CH imines), 1600.92 (NH bend.), 1475.54 (C=N *str.*), 1408.04 (C-N *str.*), 1319.31 (C=S *str.*), 1255.66 (-OCH_2), 665.44 (C-S, *str.*), 420.48 (Ru-N and Ru-S); ^{1}H NMR (DMSO-d_6, 300 MHz) δ (ppm): δ 13.00 (1H, s, NH), 7.95 (2H, s, NH_2), 6.79 (2H, d, =CH), 5.46 (2H, s, -OCH_2); ^{13}C NMR (DMSO-d_6, 300 MHz) δ (ppm): 193.84 (C=S), 136.85 (C=N), 161.78 (C-NO_2), 128.39 ($COCH_2$), 121.70 (=CH), 115.27 (=CH). ESI/MS (methanol) *m/z*: 875.00 (875.40, M^+). Anal. calcd. (found) % for $C_{45}H_{41}N_8O_3SRu$: C, 59.36 (59.26); H, 4.54 (4.50); N, 12.31 (12.28); S, 3.52 (3.48).

[ZnCl(H$_2$O)HL1]Cl (ML4): Complex **ML4** was synthesized by addition of ligand HL1 (0.1 mol, 0.359 g) and $ZnCl_2$ (0.1 mol, 0.136 g) in methanol (100 mL) was added and stirred for 2 h. The yellow-coloured product formed was filtered, washed with methanol, followed by absolute ether and dried. The complex was recrystallized in methanol and dried in vacuum. Colour: Yellow. Yield: (115.8 mg, 59%); m.p.: > 250 ºC; UV-Vis (Methanol, 10^{-3} M, λ_{max} nm): 250, 320, 360, FTIR (KBr, ν_{max}, cm^{-1}): 370.55 (Zn-Cl), 436.90 (Zn-N), 651.00 (Zn-S).^{1}H NMR (DMSO-d_6, 300 MHz) δ (ppm): 7.56 (s, 2H, NH_2), 7.80 (s, 1H, NH), 7.85-8.62 (m, 8H, ArH), ESI/MS (methanol) *m/z*: 475.46 (475.86, M^+). Anal. calcd. (found) % for $C_{16}H_{14}N_4O_2SCl_3Zn$: C, 37.38 (37.28); H, 2.74 (2.76); N, 10.90 (10.20); S, 6.24 (6.21); Zn, 12.72 (12.82).

[ZnCl(H$_2$O)HL2]Cl (ML5): Complex **ML5** was synthesized by addition of ligand HL2 (0.001 mol, 0.342 g) and $ZnCl_2$ (0.001 mol, 0.136 g) in methanol (100 mL) and refluxed for 2 h.

The volume of the resulting solution was reduced to 20mL using rotatory evaporator. The yellow-coloured product formed was filtered and recrystallized in methanol washed with ether and dried in vacuum. Colour: Yellow. Yield: (115.8 mg, 59%); m.p.: > 250 ºC; FT-IR (KBr, ν_{max}, cm^{-1}): 378.06 (Zn-Cl), 509.23 (Zn-N), 700.19 (Zn-S). ^{1}H NMR (DMSO-d_6, 300 MHz) δ (ppm): 3.91 (s, 3H, CH_3), 5.76 (s, 2H, CH_2), 6.82 (s, 2H, NH_2), 6.87 (s, 1H, NH), 8.61-6.82 (m, ArH); UV-Vis (ethanol, 10^{-3} M, λ_{max}, nm): 250, 320, 380; ESI/MS (methanol) *m/z*: 471.51 (471.63, M^+) Anal. calcd. (found) % for $C_{17}H_{17}N_4O_4SZnCl_2$: C, 40.06 (v); H, 3.36 (3.38); N, 10.99 (10.72); S, 6.29 (12.80).

[ZnCl(H$_2$O)HL3] (ML6): To a methanol solution of ligand HL3 (0.001 mol, 0.478 g), $ZnCl_2$ (0.001 mol, 0.136 g) in methanol was added and stirred for 2 h. The yellow colour product formed was filtered, washed with methanol, followed by ether and dried *in vaccuo*. Colour: Yellow. Yield: (115.8 mg, 59%); m.p.: > 250 ºC; FT-IR (KBr, ν_{max}, cm^{-1}): 420.48 (Zn-Cl), 547.78 (Zn-N), 756.10 (Zn-S). ^{1}H NMR (DMSO-d_6, 300 MHz) δ (ppm): 5.05 (s, 2H, $OCH_2C_6H_5$), 7.40 (d, 2H, CH=CH), 7.17 (s, 2H, NH_2), 6.87 (s, 1H, NH), 8.61-6.82 (m, ArH). UV-Vis (ethanol, 10^{-3} M, λ_{max}, nm): 250, 330, 360, 410; ESI/MS (methanol) *m/z* calcd. (found): 447.55 (447.55, M^+) Anal. calcd. (found) % for $C_{23}H_{21}N_4O_4SCl_2Zn$: C, 47.16 (47.18); H, 3.61 (3.63); N, 9.56 (9.73); Cl, 12.10 (12.37); S, 5.47 (5.53); Zn, 11.16 (11.36).

RESULTS AND DISCUSSION

New thiosemicarbazones ligands (HL1-HL3) were synthesized by reacting 4-substituted benzaldehyde (Cl, OCH_3 and $OCH_2C_6H_5$) with 3-nitroacetophenones *via* condensation reaction. These ligands were further reacted with $[Ru(bpy)_2Cl_2]\cdot 2H_2O$ and zinc chloride to obtain the complexes ML1-ML6. All the complexes were air stable and soluble in organic solvents but insoluble in water. The composition and structures of the newly synthesized ligands and their complexes were confirmed on the basis of physical, analytical and spectroscopic techniques. The conductivities of metal complexes ML1- ML3 were electrolytic in nature while ML4-ML6 were non-electrolytic.

Optimized geometry of metal complexes: The gas phase geometries of the compounds were optimized using density functional theory (DFT) B3LYP functional and LANL2DZ basis set for Ru and 6-31G** basis set for rest of the atomic canters (Fig. 1). The optimized geometrical parameters are presented in Table-1. The Ru-S distance in **ML1** is 2.754, **ML2** is 2.565 and **ML3** are 2.228, which is significantly shorter than the reported crystal structure of a similar type of the moieties [40]. Further, the Ru-N distance in **ML3** is shorter than the **ML1** and **ML2**, might be due to the benzyloxy group. While the bond angle ∠Ru-S-C in ML3 is 89.3º, which is greater than the **ML1** and **ML2**.

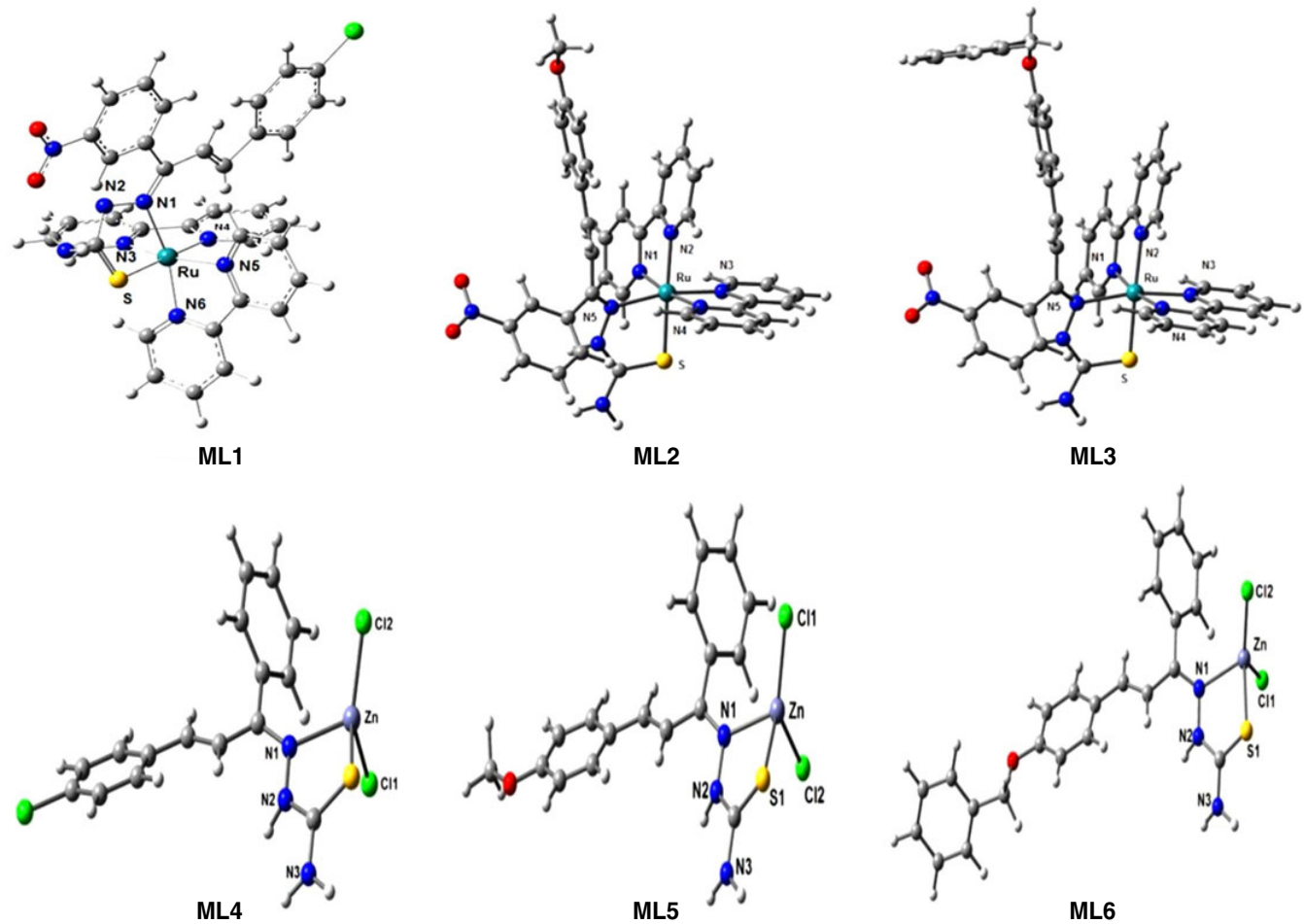

Fig. 1. Perspective optimized geometry of the complexes

TABLE-1
SELECTED OPTIMIZED GEOMETRICAL PARAMETERS FOR THE RUTHENIUM(II) COMPLEXES (BOND LENGTH (Å) AND BOND ANGLE (°)

Bond length (Å)	ML1	ML2	ML3	Bond length (Å)	ML4	ML5	ML6
Ru-S	2.574	2.565	2.228	Ru-N5	2.126	2.125	1.957
Ru-N1	2.142	2.141	1.986	Zn-Cl1	2.247	2.250	2.245
Ru-N2	2.120	2.119	1.953	Zn-Cl2	2.293	2.296	2.283
Ru-N3	2.073	2.074	1.963	Zn-S	2.560	2.561	2.562
Ru-N4	2.107	2.108	1.967	Zn-N	2.258	2.247	2.267
Bond angle (°)	**ML1**	**ML2**	**ML3**	**Bond angle (°)**	**ML4**	**ML5**	**ML6**
Ru-S-C	77.78	77.95	89.38	Cl1-Zn-Cl2	132.77	132.10	130.96
Ru-N1-C	108.25	108.12	100.39	Cl1-Zn-S	112.53	112.40	112.05
Ru-N2-C	114.71	114.75	115.67	Cl1-Zn-N	115.872	116.32	115.32
Ru-N3-C	116.12	116.12	115.64	Cl2-Zn-S	106.49	106.44	107.46
Ru-N4-C	115.77	115.21	116.25	Cl2-Zn-N	97.53	98.00	100.06
Ru-N5-C	115.17	117.71	116.26	–	–	–	–

Spectroscopic characterization studies: The IR spectra of the chalcones-thiosemicarbazones (HL1-HL3) show the bands at about 1381 and 1340 cm^{-1}, attributed to the ν(C=S) [41-44]. Further, the strong band appears at 2950-2850 cm^{-1}, which can be assigned to NH stretching. Additionally, a strong band in the range 1513-1507 cm^{-1} is assigned to ν(C=N), suggestive of the condensation of chalcones with thiosemicarbazide. In IR spectra of the metal complexes, the ν(C=N) band is shifted to lower frequencies by 40-15 cm^{-1}, which imply the coordination of the azomethine nitrogen to the ruthenium center. The new band appearing around 540-515 cm^{-1} corresponds to ν(M-N) [45]. These bands were shifted to lower wavenumbers in complexes ML1-ML6 and lower shift can be assign to the thio group ν(C=S) stretching and bending modes of vibrations and to the coordination of sulfur atom to metal ion [41,42,45]. The presence of absorption band between 1576-1560 cm^{-1}, 1123-1106 cm^{-1}, corresponds to ν(NH_2), ν(N=N), respectively. It is further confirmed by the appearance of new additional bands in the regions 1105-1056 cm^{-1} and 768-736 cm^{-1} due to the bipyridine ring –C–H and –C=N stretching vibrations, respectively. The bands corresponding to ν(Ru–N) and ν(Ru–S) vibrations appear in the range of 520-495 cm^{-1} and 450-418 cm^{-1}, respectively and show a good agreement with computed frequencies given in Table-2 along with their potential energy distribution.

The ^{1}H NMR spectra of ligands HL1-HL3 were recorded in DMSO-d_6, displayed signals at δ 11.04-11.38 and δ 4.40-4.48 ppm, which can be ascribed to NH and NH_2 protons, respectively. The resonances arising at around δ 6.778.28 ppm can be arising because of the aromatic protons. The signal corresponding to OCH_3 and OCH_2 protons in HL2 and HL3 appears at δ 2.55-3.42 and 5.0 ppm [43]. After coordination, the signals at δ 11.00-11.32 ppm corresponding to NH proton neither shifted nor disappeared. This indicates that the deprotonation of ligands (NH) did not occur during coordination to the Ru(II) center in the metal complexes **ML1**, **ML2** and **ML6**. Further, the disappearance of NH proton in **ML3**, **ML4** and **ML5** supports the coordination of C-S to the metal center. The presences of 2,2′-bipyridyl in the metal complexes **ML1-ML3** have been confirmed by the appearance of signals at δ 7.50, 7.70, 8.15 and 8.85 ppm. Presence of two doublets at δ 5.04 ppm is due to methylene (-CH_2). Two multiplet signals of eight protons observed for the complexes at δ ~ 7.58 ppm and δ 8.31 ppm have been assigned to bipyridyl protons [44]. Furthermore, the ^{13}C NMR of all the ligand and its metal complexes were found to be in the range in which resonances pertaining to C=S, C=N, C-NO_2 appears at ~187-190, 155-148 and 140-144, respectively.

Electronic absorption: The electronic absorption spectra of ligands and their corresponding Ru(II) complexes are shown in Fig. 2. In ligands, the bands at 374, 319 and 239 nm can be accredited to benzothiazolylhydrazone moiety. The band obtained at 370 nm is assigned to the transition of azomethine (C=N) group. To have insight into the nature of electronic transitions in all three complexes their gas phase geometries were optimized (vide infra). In the case of complexes, the absorption bands at 316, 386 and 223 nm are arising because of the transitions occurring in the ligands [46]. In particular, the band at ~290-300 nm is having dominant contribution from transition involving bipyridyl moieties. The calculated spectrum of **ML2** was observed at 503, 361, 292, 244 and 206 nm. The Lowest transitions at 475 nm (HOMO-LUMO) are MLCT transitions from ruthenium to chalcone thiosemicarbazones

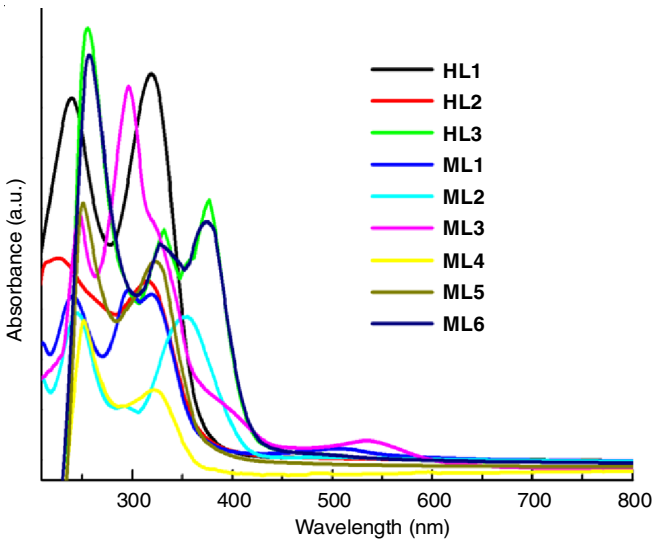

Fig. 2. UV-vis spectra of metal complexes

TABLE-2
SOME SELECTED VIBRATIONAL MODES ALONG WITH PED OF METAL COMPLEXES

Complex	Calculated wavenumber	Experimental wavenumber	Assignment
ML1	1101	1106	τ(C24-C22-N39-Ru78)21
	941	959	τ_{out}(C22-Ru78-C21-N39)13
	878	832	τ_{out}(C22-Ru78-C21-N39)20
	726	740	τ_{out}(Ru78-C1-C2-N20)10
	640	720	τ(C31-N40-Ru78-N20)13
	621	704	τ(C50-C49-N48-Ru78)15
	599	595	ν(Ru78-N48)12
ML2	469	481	τ_{out}(C50-C49-N69-Ru70)10
	446	434	ν(Ru70-N67)15
ML3	843	843	τ_{out}(N68-Ru70-N67-C30)12
	833	833	τ(N68-Ru70-N67-C30)12
	515	520	τ(C50-C49-N69-Ru70)21
	495	550	τ(C50-C49-N69-Ru70)11 + τ_{out} (C49-Ru70-C48-N69)15
	470	500	ν(Ru70-N67)23 + $\tau_{ou\ t}$(C53-N68-Ru70-N67)13
	467	450	ν(Ru70-N67)11 + τ_{out}(C54-Ru70-C53-N68)11
ML4	898	894	β(Zn34-N12-C11)16
	825	830	τ_{out}(N27-Zn34-C11-N12)19
	466		ν_{as} (Zn34-Cl36)18 + τ(Zn34-N12-C11-C13)11
	464		τ(C32-N27-N12-Zn34)23
	458	508	ν(Zn34-Cl36)25
	426	436	τ(Zn34-N12-C11-C13)11
	379	370	ν_{as} (Zn34-Cl36)16
ML5	464	509	τ_{out}(Zn34-N12-C11-C13)13
	427	441	τ(Zn34-N12-C11-C13)17
	372	378	β_{out} (Cl35-Zn34-Cl36)10 + τ_{out}(Cl35-N12-Cl36-Zn34)36
	272	-	ν_{as} (Zn34-N12)26
ML6	917	960	β (Zn34-N12-C11)20
	714	719	τ_{out}(N27-Zn34-C11-N12)10
	470	500	τ(Zn34-N12-C11-C13)12
	466	450	τ(C32-N27-N12-Zn34)10
	322	-	ν(Zn34-Cl36)17 + β (Cl35-Zn34-Cl36)19
	308	-	ν(Zn34-Cl36)20
	305	-	ν(Zn34-Cl35)43
	279	-	τ_{out}(Cl36-N12-S33-Zn34)40
	230	-	ν(Zn34-Cl36)33 + ν_{as}(Zn34-Cl35)17 + τ_{out}(Cl36-N12-S33-Zn34)19

and or 2,2′-bipyridine. However, the ground states transition at 501 nm (**ML2**) was expected to arise from bipyridine ligand [47]. The comparison between the observed and calculated spectral values reveals that the observed spectra nearly closer to the calculated values in the range 475-520 nm, which may be ascribed as MLCT transitions while other high energy transitions are of intra-ligand charge transitions.

Biological evaluation: The initial anti-mycobacterial activity screening performed at 100 μM with compounds **HL1**, **HL2**, **HL3**, **ML1**, **ML2** and **ML3** and showed a reduction of fluorescence in all the treated cultures. The optimized molecular structures of the Ru(II) based complexes showed more than 90% reduction in fluorescence as was observed in **HL2**, **HL3** and **ML3** treated cultures (Fig. 3A). Also, **ML3** and **HL3** showed good inhibition of treated *Mtb*-Ra cultures even at 25 μM concentration (Fig. 4). However, compounds **ML4**, **ML5** and **ML6** showed lower activity (Fig. 3B). The potential activity shown by **HL3** and **ML3** cultures showed them to be promising compounds that may be further optimized for improved anti-mycobacterial activity. The MABA based DST using redox active dyes for colourimetric/fluorescence measurements are fast, reliable as well as less costly and easy to perform, compared to MGIT and BACTEC [48-54]. The Alamar blue is a fluorescent redox active dye and its active component resazurin is non-fluorescent in its oxidized form and its reduction by cellular redox enzymes leads to the formation of highly fluorescent compound (resorufin). This leads too many fold increases in fluorescence of solution when cells are active metabolically, however, in MABA based drug screening assays when cells are inhibited with compounds having inhibitory activity, then compared to untreated control, not much increase of fluorescence is observed in treated samples. This confirms that the inhibition as in untreated control fluorescence increases over a period of time till all resazurin is converted to resorufin. In the present study, both **HL3** and **ML3** showed the promising activity, which can be further optimized.

Antimicrobial activity: The antimicrobial activities of samples were checked by Kirby-Bauer disc diffusion method.

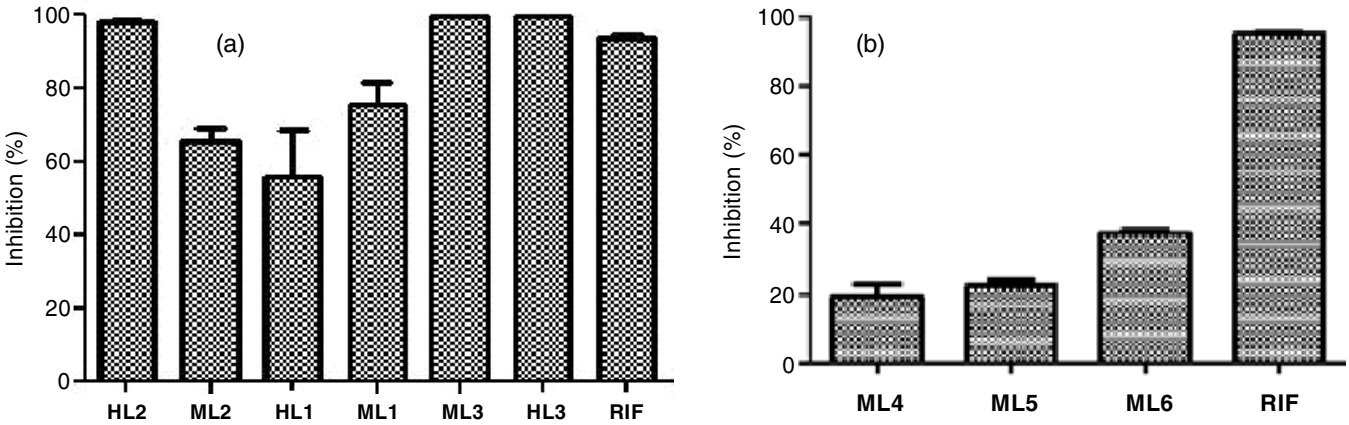

Fig. 3. Inhibition of *Mycobacterium tuberculosis* H37Ra at a fixed concentration of 100 μM. The RIF refers to rifampicin at 5 μg/mL concentration. The fluorescence was recorded at 535/595 excitation/emission

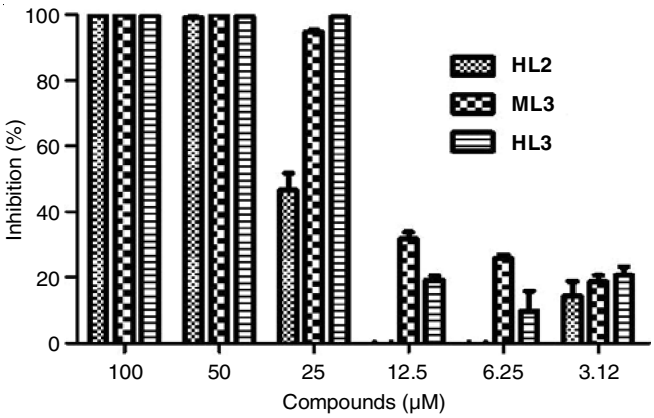

Fig. 4. MIC determination of **HL2**, **ML3** and **HL3** by MABA assay. The compounds were diluted from 100 μM to 3.12 μM concentrations and growth was measured after incubating plates for 5 days followed by addition of 25 μL resazurin (0.03%) and incubating again for 5 h. The fluorescence was recorded at 535/595 excitation/emission

MHA medium plates surface were inoculated by spreading with 100 μL of log phase cultures (OD adjusted to McFarland unit (0.5) concentration of *Bacillus subtilis*) followed by placing the discs containing 20 μL volume of 200 μg/mL sample. DMSO (20 μL/disc) was used as vehicle control. The plates were incubated at 37 ºC for 24 h. This protocol is based on the ability of antimicrobial agent to diffuse into the agar medium and inhibit the growth of the microorganism being evaluated. This leads to formation of a clear zone of inhibition, which is measured to estimate the growth inhibition.

Electronic properties and global reactivity parameters: The HOMO and LUMO plots with an energy band gap of all metal complexes are given in Fig. 5. The band gap of **ML1**, **ML2**, **ML3**, **ML4**, **ML5** and **ML6** were 3.108, 2.840, 2.518, 3.388, 3.505 and 3.494 eV, respectively. Among all of these complexes **ML3** has smallest value of energy band-gap. This may suggest that **ML3** is chemically more reactive than other complexes and **ML5** has a high bandgap among all of these corresponds to less chemically reactive. The global reactivity parameters like chemical potential, electronegativity, hardness, softness and electrophilicity index can be defined within the framework of DFT using B3LYP/6-311G** and LANL2DZ level of theory. Ionization potential (IP) and electron affinity (EA) are interpreted by difference in ground state energy between the cationic and neutral system and difference in ground state energy between neutral and anionic system *i.e.* IP = E (N–1)–E(N) and EA = E(N)–E(N+1). Chemical descriptors give an important understanding of chemical reactivity and hence biological activity of the molecule. The chemical hardness gives measurement of the stability of a molecule, while the strength to attract electrons in a chemical bond is described by electronegativity and mathematically it can be defined by $\chi = (IP+EA)/2$. The global softness ($S = 1/\eta$) is expressed by the reciprocal of chemical hardness. The global electrophilicity index is related with hardness and electronegativity as $\omega = \mu^2/2\eta$ and related to the lowering of energy due to maximal electron flow between donor and acceptor [55,56]. All the parameters with formula are listed in Table-3.

TABLE-3
GLOBAL REACTIVITY PARAMETERS OF METAL COMPLEXES

Complex	Ionization potential (eV) $IP= -E_{HOMO}$	Electron affinity (eV) $EA= -E_{LUMO}$	Electronic chemical potential $\mu = -(IP + EA)/2$	Electronegativity (eV) $\chi = (IP + EA)/2$	Chemical hardness (eV) $\eta = (IP-EA)/2$	Global softness (eV) $S = 1/\eta$	Global electrophilicity index (eV) $\omega = \chi^2/2\eta$
ML1	10.651	7.543	-9.097	9.097	1.554	0.643	26.626
ML2	10.354	7.514	-8.934	8.934	1.42	0.704	28.104
ML3	9.972	7.453	-8.712	8.712	1.259	0.794	30.142
ML4	6.723	3.335	-5.029	5.029	1.694	0.590	7.464
ML5	6.525	3.020	-4.772	4.772	1.752	0.570	6.498
ML6	6.480	2.986	-4.733	4.733	1.747	0.572	6.411

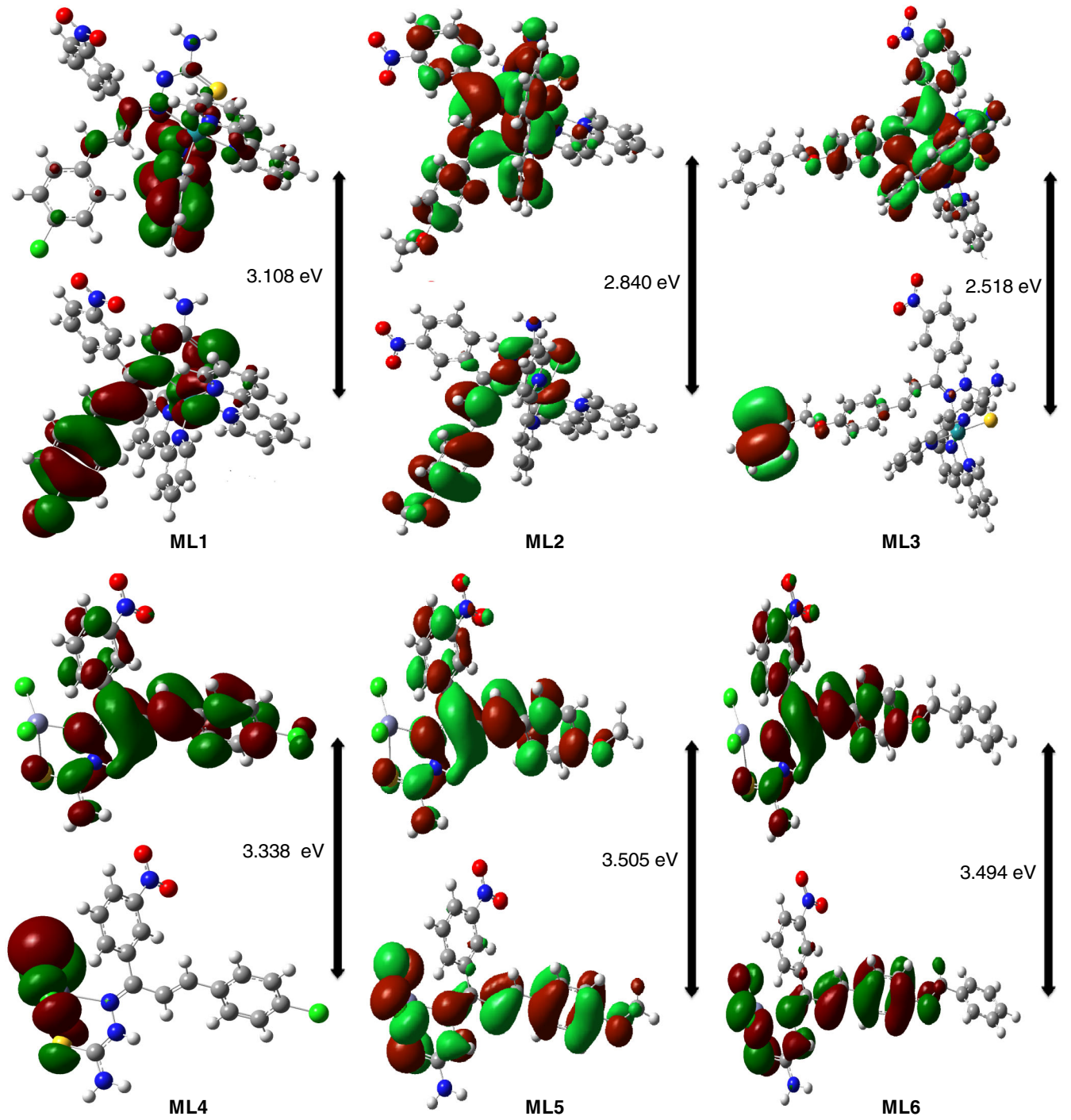

Fig. 5. HOMO LUMO plot of all metal complexes using DFT/B3LYP/6-31G** and LANL2DZ level of theory

The calculated value of chemical hardness of ML5 is 1.752 eV, which is highest among all the metal complexes. As we know chemical hardness is also corresponded with HOMO-LUMO gap. If one molecule has high or low HOMO-LUMO gap, it is a hard or a soft molecule. The molecule with least HOMO-LUMO gap is most reactive and **ML3** having lowest value of hardness as well as HOMO-LUMO gap, possess high reactivity which supports the promising biological activity of this complex. The metal complex **ML1** has high value of ionization potential and electronegativity reflecting its most electronegative behaviour amongst all of the metal complexes.

Electric moments: The dipole moment and polarizability of metal complexes have been calculated at DFT-B3LYP/6-311G** and LANL2DZ level of theory and tabulated in Table-4. Dipole moment is a significant property which is first and foremost used to study the intermolecular interactions involving non-bonded type dipole-dipole interaction. The higher the dipole moment, the stronger will be the intermolecular interactions. In present case, the calculated total dipole moment of complex **ML6** is 19.0353 Debye, which is higher than other metal complexes. The calculated value of mean polarizability (α_{mean}) of **ML1**, **ML2**, **ML3**, **ML4**, **ML5** and **ML6** were found

TABLE-4
DIPOLE MOMENT AND POLARIZABILITY OF METAL COMPLEXES
CALCULATED AT DFT-B3LYP/6-311G** LANL2DZ LEVEL OF THEORY

Complex	Dipole moment (Debye)	Polarizability (a.u.)						
		α_{xx}	α_{xy}	α_{yy}	α_{xz}	α_{yz}	α_{zz}	α_{o}
ML1	10.6295	562.429	-51.0036	652.511	60.6271	44.7917	645.590	620.176
ML2	9.7778	648.328	880.098	611.548	700.855	-983.961	609.512	623.130
ML3	14.6902	618.958	-90.6779	724.052	34.1037	-122.635	794.266	712.425
ML4	14.5174	259.212	81.8456	317.787	83.5352	20.3147	385.891	320.963
ML5	18.1067	253.764	78.8094	322.002	-86.2803	-28.5600	426.427	334.064
ML6	19.0353	284.054	57.7895	378.122	91.8611	56.5557	554.555	405.577

to be 620.176, 623.130, 712.425, 320.963, 334.064 and 405.577 a.u., respectively. High dipole moment and mean polarizability value of complex **ML3**, which corresponds that small energy band gap may put into its bioactivity as a highly polarizable ligand is likely to interact more strongly than a weakly polarizable ligand to its mark. These electric moments values are in consonance with the biological activity of the metal complexes.

Molecular docking studies: Penicillinco, here to the penicillin binding proteins (PBPs), PBPs catalyze the peptidoglycan synthesis, which includes three enzymatic steps: (i) glycosyltransferase (GT) polymerizing the glycan strand by using the substrate, lipid II, (ii) *trans*-peptidase (TP) that crosslinks these strands through their peptide residues, (iii) D-alanine carboxypeptidase, playing a regulatory role [57]. The penicillin antibiotics inhibit the TP active site of PBPs, which contains catalytic serine. The active site of serine breaks down the lactam ring of the β-lactam antibiotics by the nucleophilic attack developing into a covalently bound inhibitor [58]. There are seven different types of PBPs (PBP 1a, 1b, 2a, 2b, 3, 4, 5) [59]. PBP 2a is the target of choice for antibacterial chemotherapy as it is important for cell viability. Antibiotics usable in human therapy do not particularly inhibit GT activity [60]. In current work, *S. aureus* PBP2a (PDB ID 5 m18) has been sort out for *in silico* study. Ser 403 the docking and binding energy estimations are carried out by AutoDock4 [51]. Figures were prepared by applying Biovia Discovery Studio visualization. Mixed-ligand metal complex with ligand protects the compound from hydrolysis of β-lactam ring by β-lactamase, a penicillin resistance factor. Thus, metal complexes overcome the penicillin resistance due to β-lactamase. The differential values of dipole moment of the complex (magnitude and orientation) results in the differential PBP 2a (5m18) binding affinity of the complexes and hence the antimycobacterial effect may be due to the differential values of dipole moment of the complex (magnitude and orientation) (Table-5). Binding affinities of the mixed-ligand metal complex were improved and metal toxicity is also suppressed by complex formation with ligand. The docking analysis and hydrogen bond interactions are shown in Figs. 6 and 7.

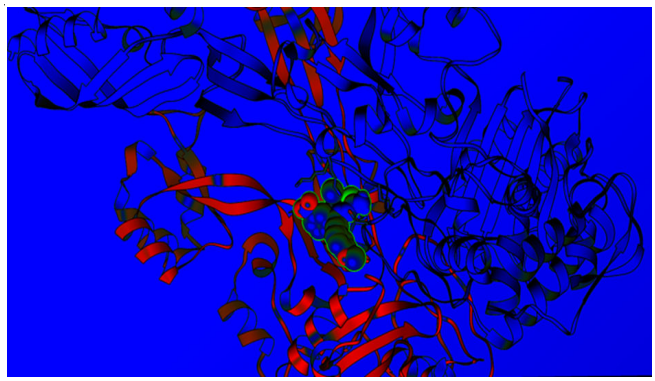

Fig. 6. Active site of penicillin binding protein 5m18 A (represented in ribbon model). Ligand Zn-mixed ligand complex binding to the active site

Conclusion

In summary, three ruthenium bipyridine and three zinc complexes of chalcone-thiosemicarbazones ligands have been synthesized and characterized. The study of antimycobacterial properties of these complexes suggested that the nature of functional group at the *para*-position of the aromatic ring in the ligands plays pivotal role in tuning the electronic properties of the resulting complexes which in turn varied their antimycobacterial properties. In all syntheized metal complexes, the C=N and C=S groups of the thiosemicarbazones were found to be coordinated to the Ru(II) center. Such systems may be interesting as like rifampicin these ligands also comprises of C=N and NH which are responsible for antimycobacterial activities in valued association with the functional group at

TABLE-5
DOCKING RESULTS OF Ru COMPLEXES (**ML1**, **ML2**, **ML3**) AND Zn COMPLEXES (**ML4**, **ML5**, **ML6**)

Complex	Binding energy	Inhibition constant	Intermolecular energy	Total energy	Torsional energy	Electrostatic energy
ML1	-4.29	712.75	7.04	4.63	2.74	0.47
ML2	-3.49	2.76	6.78	4.34	3.29	0.17
ML3	-3.43	3.04	7.00	4.49	3.57	0.65
ML4	-5.73	63.80	7.22	0.95	1.49	0.13
ML5	-5.26	139.86	7.05	1.06	1.79	0.92
ML6	-7.56	2.89	10.24	1.62	2.68	3.02

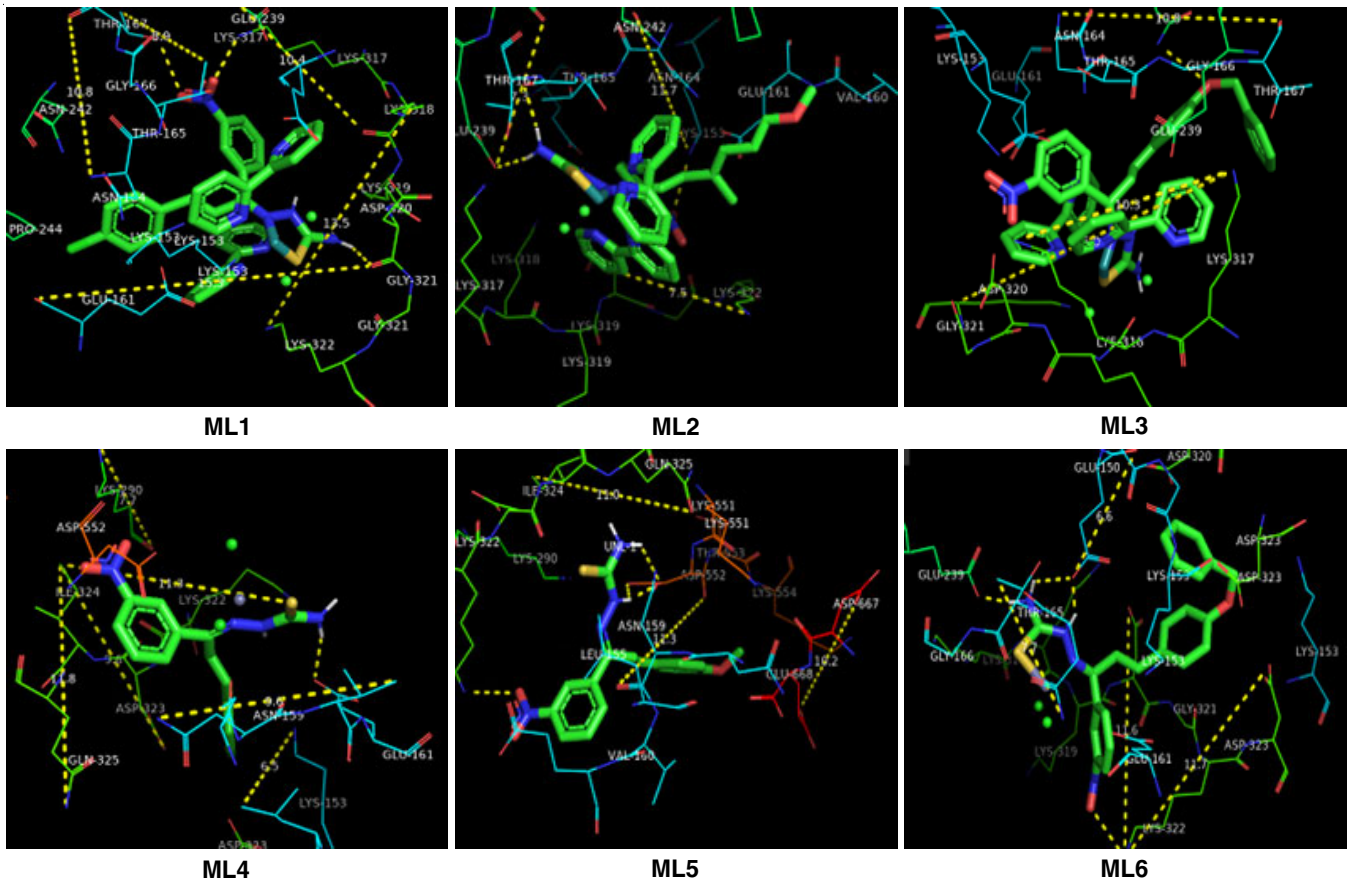

Fig. 7. Receptor ligand interactions of mixed-ligand complexes of (a) ruthenium (**ML1**, **ML2**, **ML3**) and (b) zinc (**ML4**, **ML5**, **ML6**) in the active site of penicillin binding protein (5m18 A)

the *para*-position of the aromatic ring. Such investigations will pave a new path to develop analogous Ru(II) based complexes can offer certain medicinal properties. The notable binding energies obtained by performing molecular docking would suggest that especially the complexes with transitional metals could be more potent biocompounds than the ligand.

ACKNOWLEDGEMENTS

The author gratefully acknowledges financial support from Research and Development, S. No.47/2021/606/70-4-2021-4 (56)/2020, Uttar Pradesh Government, Lucknow, India for providing the financial support. The authors are also thankful to SAIF, CSIR and DST-PURSE, Department of Chemistry, Lucknow University, India for providing the spectral facilities.

CONFLICT OF INTEREST

The authors declare that there is no conflict of interests regarding the publication of this article.

REFERENCES

1. G. Subramanian, R. Mural, S.L. Hoffman, J.C. Venter and S. Broder, *Mol. Diagn.*, **6**, 243 (2001); https://doi.org/10.2165/00066982-200106040-00006
2. P.S. Kim and S. Swaminathan, *J. Int. AIDS Soc.*, **24**, e25698 (2021); https://doi.org/10.1002/jia2.25698
3. A. Gómez-Suárez, D.J. Nelson, D.G. Thompson, D.B. Cordes, D. Graham, A.M.Z. Slawin and S.P. Nolan, *Beilstein J. Org. Chem.*, **9**, 2216 (2013); https://doi.org/10.3762/bjoc.9.260
4. J.M.S. Cardoso, A.M. Galvão, S.I. Guerreiro, J.H. Leitão, A.C. Suarez and M.F.N.N. Carvalho, *Dalton Trans.*, **45**, 7114 (2016); https://doi.org/10.1039/C6DT00099A
5. M.J. Clarke, F. Zhu and D.R. Frasca, *Chem. Rev.*, **99**, 2511 (1999); https://doi.org/10.1021/cr9804238
6. T.B. Hadda, M. Akkurt, M.F. Baba, M. Daoudi, B. Bennani, A. Kerbal and Z.H. Chohan, *J. Enzyme Inhib. Med. Chem.*, **24**, 457 (2009); https://doi.org/10.1080/14756360802188628
7. R.I. Kureshy and N.H. Khan, *Polyhedron*, **12**, 195 (1993); https://doi.org/10.1016/S0277-5387(00)81627-7
8. A. Jabłońska-Wawrzycka, P. Rogala, S. Michalkiewicz, M. Hodorowicz and B. Barszcz, *Dalton Trans.*, **42**, 6092 (2013); https://doi.org/10.1039/c3dt32214a
9. J. Chakravarty and S. Bhattacharya, *Polyhedron*, **15**, 1047 (1996); https://doi.org/10.1016/0277-5387(95)00362-2
10. I. Mantasha, M.K. Raza, M. Shahid, A. Ansari, M. Ahmad and I.M. Khan, *Appl. Organomet. Chem.*, **33**, 5006 (2019); https://doi.org/10.1002/aoc.5006
11. M.N. Ahamad, M. Shahid, A. Ansari, M. Kumar, I.M. Khan, M. Ahmad, R. Rahisuddin and R. Arif, *New J. Chem.*, **43**, 7511 (2019); https://doi.org/10.1039/C9NJ00228F
12. F. Sama, M. Raizada, M. Ashafaq, M.N. Ahamad, I. Mantasha, K. Iman, M. Shahid, R. Rahisuddin, R. Arif, N.A. Shah and H.A.M. Saleh, *J. Mol. Struct.*, **1176**, 283 (2019); https://doi.org/10.1016/j.molstruc.2018.08.081
13. I. Mantasha, M. Shahid, M. Ahmad, R. Rahisuddin, R. Arif, S. Tasneem, F. Sama and I.A. Ansari, *New J. Chem.*, **43**, 622 (2019); https://doi.org/10.1039/C8NJ04122A
14. S.B. Mohamed, T.A. Adlan, N.A. Khalafalla, N.I. Abdalla, Z.S.A. Ali, A. Munir KA, M.M. Hassan and M.-A.B. Elnour, *Evol. Bioinform. Online*, **15**, 1 (2019); https://doi.org/10.1177/1176934319864945

15. M.M. Miyachiro, C. Contreras-Martel and A. Dessen, *Subcell. Biochem.*, **93**, 273 (2019); https://doi.org/10.1007/978-3-030-28151-9_8
16. T.P. Cushnie, N.H. O'Driscoll and A.J. Lamb, *Cell. Mol. Life Sci.*, **73**, 4471 (2016); https://doi.org/10.1007/s00018-016-2302-2
17. M. Nguyen-Distèche, M. Leyh-Bouille and J.M. Ghuysen, *Biochem. J.*, **207**, 109 (1982); https://doi.org/10.1042/bj2070109
18. H.F. Chambers, *J. Infect. Dis.*, **179(s2)**, S353 (1999); https://doi.org/10.1086/513854
19. W. Kohn and L.J. Sham, *Phys. Rev.*, **140(4A)**, A1133 (1965); https://doi.org/10.1103/PhysRev.140.A1133
20. A.D. Becke, *J. Chem. Phys.*, **98**, 5648 (1993); https://doi.org/10.1063/1.464913
21. C. Lee, W. Yang and R.G. Parr, *Phys. Rev. B Condens. Matter*, **37**, 785 (1988); https://doi.org/10.1103/PhysRevB.37.785
22. B. Miehlich, A. Savin, H. Stoll and H. Preuss, *Chem. Phys. Lett.*, **157**, 200 (1989); https://doi.org/10.1016/0009-2614(89)87234-3
23. P.J. Hay and W.R. Wadt, *J. Chem. Phys.*, **82**, 270 (1985); https://doi.org/10.1063/1.448799
24. W.R. Wadt and P.J. Hay, *J. Chem. Phys.*, **82**, 284 (1985); https://doi.org/10.1063/1.448800
25. P.J. Hay and W.R. Wadt, *J. Chem. Phys.*, **82**, 299 (1985); https://doi.org/10.1063/1.448975
26. M.J. Frisch, G. Trucks, H.B. Schlegel, G.E. Scuseria, M.A. Robb, J. Cheeseman, G. Scalmani, V. Barone, B. Mennucci, Benedetta, G.A. Petersson, H. Nakatsuji, M. Caricato, X. Li, H.P. Hratchian, A.F. Izmaylov, J. Bloino, G. Zheng, J. Sonnenberg, M. Hada and D. Fox, Gaussian 09 Revision A.1. Gaussian Inc. (2009).
27. A.P. Scott and L. Radom, *J. Phys. Chem.*, **100**, 16502 (1996); https://doi.org/10.1021/jp960976r
28. P. Pulay, G. Fogarasi, G. Pongor, J.E. Boggs and A. Vargha, *J. Am. Chem. Soc.*, **105**, 7037 (1983); https://doi.org/10.1021/ja00362a005
29. Æ. Frisch, H.P. Hratchian, R.D. Dennington II, T.A. Keith, J. Millam, A.B. Nielsen, A.J. Holder and J. Hiscocks, GaussView version 5.0, Gaussian, Inc. (2009).
30. M.H. Jamroz, Vibrational Energy Distribution Analysis: VEDA 4 Program Warsaw: Poland (2004).
31. A.D. Buckingham, *Adv. Chem. Phys.*, **12**, 107 (1967); https://doi.org/10.1351/pac198052102253
32. G.M. Morris, R. Huey, W. Lindstrom, M.F. Sanner, R.K. Belew, D.S. Goodsell and A.J. Olson, *J. Comput. Chem.*, **30**, 2785 (2009); https://doi.org/10.1002/jcc.21256
33. H.M. Berman, J. Westbrook, Z. Feng, G. Gilliland, T.N. Bhat, H. Weissig, I.N. Shindyalov and P.E. Bourne, *Nucleic Acids Res.*, **28**, 235 (2000); https://doi.org/10.1093/nar/28.1.235
34. M.D. Hanwell, D.E. Curtis, D.C. Lonie, T. Vandermeersch, E. Zurek and G.R. Hutchison, *J. Cheminform.*, **4**, 17 (2012); https://doi.org/10.1186/1758-2946-4-17
35. L. Schrödinger, The PyMOL Molecular Graphics System (2010).
36. E. Pahontu, M. Proks, S. Shova, G. Lupascu, D.-C. Ilies, S.-F. Bărbuceanu, L.-I. Socea, M. Badea, V. Pãunescu, D. Istrati, A. Gulea, D. Drăgănescu and C.E.D. Pîrvu, *Appl. Organomet. Chem.*, **33**, 5185 (2019); https://doi.org/10.1002/aoc.5185
37. J.C. Palomino, A. Martin, M. Camacho, H. Guerra, J. Swings and F. Portaels, *Antimicrob. Agents Chemother.*, **46**, 2720 (2002); https://doi.org/10.1128/AAC.46.8.2720-2722.2002
38. J.C. Palomino, A. Martin and F. Portaels, *J. Clin. Microbiol.*, **8**, 754 (2007); https://doi.org/10.1111/j.1469-0691.2007.01698.x
39. M.J. Clarke, *Coord. Chem. Rev.*, **236**, 209 (2003); https://doi.org/10.1016/S0010-8545(02)00312-0
40. B. Ghosh, P. Adak, S. Naskar, B. Pakhira, P. Mitra, R. Dinda and S.K. Chattopadhyay, *Inorg. Chim. Acta*, **459**, 1 (2017); https://doi.org/10.1016/j.ica.2017.01.011
41. M. Maganarin, A. Bergamo, M.E. Carotenuto, S. Zorzet and G. Sava, *Anticancer Res.*, **20(5A)**, 2939 (2000).
42. M. Cocchietto and G. Sava, *Pharmacol. Toxicol.*, **87**, 193 (2000); https://doi.org/10.1034/j.1600-0773.2000.d01-73.x
43. S. Zorzet, A. Sorc, C. Casarsa, M. Cocchietto and G. Sava, *Met. Based Drugs*, **8**, 1 (2001); https://doi.org/10.1155/MBD.2001.1
44. J.G. Da Silva, C.C.H. Perdigão, N.L. Speziali and H. Beraldo, *J. Coord. Chem.*, **66**, 385 (2013); https://doi.org/10.1080/00958972.2012.757762
45. R. Gagliardi, G. Sava, S. Pacor, G. Mestroni and E. Alessio, *Clin. Exp. Metast.*, **12**, 93 (1994); https://doi.org/10.1007/BF01753975
46. V. Krishnakumar and S. Seshadri, *Spectrochim. Acta A*, **68**, 833 (2007); https://doi.org/10.1016/j.saa.2006.12.067
47. S. Goel, O.P. Pandey and K. Sengupta, *Thermochim. Acta*, **133**, 359 (1988); https://doi.org/10.1016/0040-6031(88)87183-1
48. P.F. Rapheal, E. Manoj and M.R. Prathapachandra Kurup, *Polyhedron*, **26**, 818 (2007); https://doi.org/10.1016/j.poly.2006.09.091
49. I.D. Kostas, F.J. Andreadaki, D. Kovala-Demertzi, Christos Prentjas and M.A. Demertzis, *Tetrahedron Lett.*, **46**, 1967 (2005); https://doi.org/10.1016/j.tetlet.2005.02.003
50. R.K. Singh and A.K. Singh, *J. Mol. Struct.*, **1129**, 128 (2017); https://doi.org/10.1016/j.molstruc.2016.09.072
51. C.A.S.T. Vilanova-Costa, H.K.P. Porto, F.C. Pereira, A.P. de Lima, W.B. dos Santos and E.P. Silveira-Lacerda, *Biometals*, **27**, 459 (2014); https://doi.org/10.1007/s10534-014-9715-x
52. U.K. Mazumder, M. Gupta, S.S. Karki, S. Bhattacharya, S. Rathinasamy and S. Thangavel, *Chem. Pharm. Bull.*, **52**, 178 (2004); https://doi.org/10.1248/cpb.52.178
53. A.K. Singh, R.K. Singh, M. Arshad and S.K. Sahabzada, *ChemistrySelect*, **3**, 12682 (2018); https://doi.org/10.1002/slct.201802929
54. H. Sklenar and J. Jager, *Int. J. Quantum Chem.*, **16**, 467 (1979); https://doi.org/10.1002/qua.560160306
55. R.G. Parr and W. Yang, Functional Theory of Atoms and Molecules, Oxford University Press: New York (1989).
56. R.K. Roy, S. Krishnamurti, P. Geerlings and S. Pal, *J. Phys. Chem. A*, **102**, 3746 (1998); https://doi.org/10.1021/jp973450v
57. T.H. Al-Noor, R.K. Mohapatra, L.K.A. Karem, P.K. Mohapatra, M. Azam, A.A. Ibrahim, P.K. Parhi, G.C. Dash, M.M. El-Ajaily, S.I. Al-Resayes, M.K. Raval and L. Pintilie, *J. Mol. Struct.*, **1229**, 129832 (2021); https://doi.org/10.1016/j.molstruc.2020.129832
58. J.M. Ghuysen, *Trends Microbiol.*, **2**, 372 (1994); https://doi.org/10.1016/0966-842X(94)90614-9
59. J.M. Ghuysen, *Annu. Rev. Microbiol.*, **45**, 37 (1991); https://doi.org/10.1146/annurev.mi.45.100191.000345
60. P. Macheboeuf, C. Contreras-Martel, V. Job, O. Dideberg and A. Dessen, *FEMS Microbiol. Rev.*, **30**, 673 (2006); https://doi.org/10.1111/j.1574-6976.2006.00024.x